Membrane nanotubes facilitate long-distance interactions between natural killer cells and target cells

Anne Chauveau[a,b], Anne Aucher[a], Philipp Eissmann[a], Eric Vivier[b,c], and Daniel M. Davis[a,1]

[a]Division of Cell and Molecular Biology, Imperial College London, London SW7 2AZ, United Kingdom; [b]Centre d'Immunologie de Marseille–Luminy, Université de la Méditerranée, Institut National de la Santé et de la Recherche Médicale Unité Mixte de Recherche (UMR) 6312, Centre National de la Recherche Scientifique UMR6102, Campus de Luminy, 13288 Marseille, France; and [c]Hôpital de la Conception, Assistance Publique-Hôpitaux de Marseille, Baille 13005, Marseille, France

Membrane nanotubes are membranous tethers that physically link cell bodies over long distances. Here, we present evidence that nanotubes allow human natural killer (NK) cells to interact functionally with target cells over long distances. Nanotubes were formed when NK cells contacted target cells and moved apart. The frequency of nanotube formation was dependent on the number of receptor/ligand interactions and increased on NK cell activation. Most importantly, NK cell nanotubes contained a submicron scale junction where proteins accumulated, including DAP10, the signaling adaptor that associates with the activating receptor NKG2D, and MHC class I chain-related protein A (MICA), a cognate ligand for NKG2D, as occurs at close intercellular synapses between NK cells and target cells. Quantitative live-cell fluorescence imaging suggested that MICA accumulated at small nanotube synapses in sufficient numbers to trigger cell activation. In addition, tyrosine-phosphorylated proteins and Vav-1 accumulated at such junctions. Functionally, nanotubes could aid the lysis of distant target cells either directly or by moving target cells along the nanotube path into close contact for lysis via a conventional immune synapse. Target cells moving along the nanotube path were commonly polarized such that their uropods faced the direction of movement. This is the opposite polarization than for normal cell migration, implying that nanotubes can specifically drive target cell movement. Finally, target cells that remained connected to an NK cell by a nanotube were frequently lysed, whereas removing the nanotube using a micromanipulator reduced lysis of these target cells.

cell activation | immune synapses | cytotoxicity | cell motility | intercellular communication

Natural killer (NK) cells are lymphocytes that can recognize and contribute to the elimination of cells undergoing several forms of stress, such as microbial infection or tumor transformation. Activation of NK cells is regulated by engagement of a variety of inhibitory and activating receptors with cognate ligands expressed on target cells (1). NKG2D is one of the best-characterized activating receptors on NK cells and recognizes stress-induced ligands, such as MHC class I chain-related protein A (MICA), at the surface of other cells (2). At the interface between NK cells and target cells, proteins accumulate to form an immune synapse (3, 4). Signal integration from activating and inhibitory receptors at the synapse leads to the appropriate effector response (4–7).

Membrane nanotubes are membranous tethers that physically link cell bodies over long distances and can vary in specific structure, process of formation, and functional properties (8–12). Nanotubes can traffic vesicles (9, 13) or transmit calcium-mediated signals (14) and can contribute to pathological conditions [e.g., by directing the spread of viruses or prions (15–17)]. Here, we demonstrate that membrane nanotubes sustain connections between a variety of target cells and primary human NK cells or cell lines. Such NK cell nanotubes contained submicrometer

scale immune synapses and could aid NK cell-mediated cytotoxicity. These data suggest how closed-ended membrane nanotubes can contribute to immune cell function.

Results

Human NK Cells Readily Form Membrane Nanotubes. To visualize intercellular membranous tethers, NK cells labeled with a membrane dye were mixed with an equal number of differently labeled NK cells or target cells, coincubated on a fibronectin-coated glass surface, and imaged by confocal microscopy. Intercellular membrane connections between differently colored cells could not have derived from cell division and were considered as membrane nanotubes (Fig. 1 A and B and Fig. S1 A and B). Such nanotubes were not attached to the substratum, which is one of the attributes that distinguishes them from filopodia (Fig. S1C). After 45 min of coincubation, $2.4 \pm 0.4\%$, $3.6 \pm 0.5\%$, $6.3 \pm 0.9\%$, and $5.1 \pm 0.3\%$ of primary NK cells were connected to other primary NK cells, mouse mastocytoma P815, human 721.221 EBV-transformed B cells (221), and human monocyte-derived THP-1, respectively (Fig. 1C). Similarly, $3.8 \pm 0.6\%$, $2.6 \pm 0.3\%$, $7.5 \pm 1.4\%$, and $7.8 \pm 1.1\%$ of the immortal human NK cell tumor line (NKL) were connected to another NKL, P815, 221, and THP-1, respectively (Fig. S1D). Nanotube length was significantly different between primary human NK cells (11.4 ± 0.6 μm) and NKL cells (21.4 ± 1.0 μm) and could sometimes extend to >100 μm (Fig. 1D and Fig. S1E). In contrast, the length of nanotubes was invariant with different target cells (Fig. 1D and Fig. S1E), likely a reflection that most NK cell nanotubes were made up of NK cell membrane. NK cell nanotubes could also form within a 3D mimic of extracellular matrix (Fig. S1F).

Characterization of NK Cell Membrane Nanotubes. Intercellular membrane tethers can form either by actin-rich filopodial protrusions extending out from one cell to connect to a distant cell or when cells are in close contact and subsequently depart (8). Live-cell time-lapse microscopy revealed that all observed NK cell nanotubes were formed as cells departed after an initial close contact (example shown in Fig. 2A and Movie S1). Thus, instead of creating connections between cells de novo, NK cell nanotubes serve to sustain intercellular contacts over long distances.
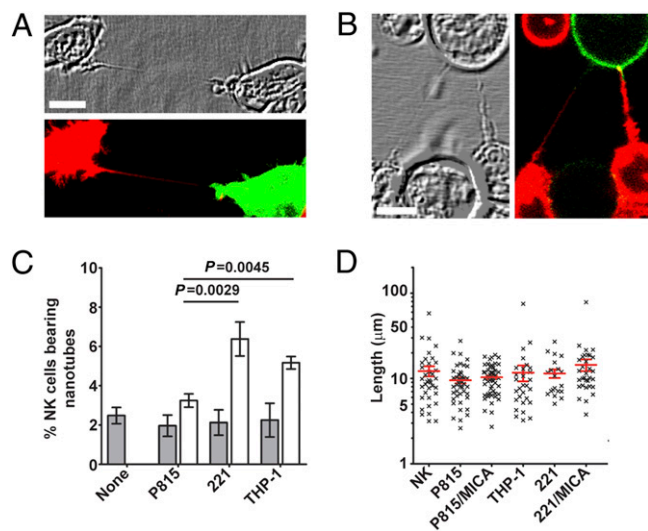
IMMUNOLOGY

Fig. 1. Human NK cells readily form membrane nanotubes. Primary cultured human NK cells labeled with membrane dye DiD (red) readily formed nanotubes with other primary NK cells labeled with 3,3′-dioctadecyloxacarbocyanine perchlorate (DiO) (green, *n* > 50) (*A*) or with P815 transfectants expressing MICA-YFP (green, *n* > 100) (*B*). (*C*) After 45 min of coculture, the frequency of nanotubes formed by primary NK cells was assessed for cells incubated alone (none) or in the presence of different target cells as indicated (*n* > 1,500 cells). Bars show the frequency of nanotubes between NK cells (shaded) and the frequency of nanotubes connecting NK cells to target cells (white). (*D*) Length of nanotubes formed between primary NK cells and different target cells (*n* > 150). (Scale bars: 10 μm.)

Cell contacts that led to nanotube formation lasted 11.4 ± 1.5 min and 10.1 ± 1.1 min for primary NK cells and NKL cells, respectively, whereas cell contacts that did not lead to nanotube formation lasted 3.7 ± 0.2 min and 4.2 ± 0.2 min, respectively (Fig. 2 *B* and *C*). Thus, brief NK cell contacts did not generally lead to nanotube formation, implicating a time-dependent process for nanotube formation. Importantly, NK cell nanotubes contained a junction, either within the nanotube or at a cell body, across which membrane-tethered or cytoplasmic fluorescent proteins could not freely diffuse (Fig. S1 *G* and *H*). Thus, NK cell nanotubes are not open-ended membrane tunnels as seen between some cell types (9).

By staining fixed cells with phalloidin, which marks f-actin, or an anti-α-tubulin mAb, f-actin was found in all NK cell nanotubes and α-tubulin was detected in 78% of them (*n* = 78) (Fig. 2 *D* and *E*). This may define a genuine heterogeneity in the cytoskeletal composition of NK cell nanotubes, or, alternatively, this could merely reflect difficulty in detection of α-tubulin in thin nanotubes. The presence of microtubules in NK cell nanotubes distinguishes them from nanotubes formed between T cells (15).

Engagement of Cognate Receptor/Ligand Pairs and Cytokine Stimulation Augment Nanotube Formation. Human NK cells formed fewer nanotubes with mouse P815 target cells compared with 221 or THP-1 (Fig. 1*C* and Fig. S1*D*), and one explanation for this would be that there are fewer cognate receptor/ligand interactions across species. Thus, to test whether nanotube formation could be influenced by the number of cognate receptor/ligand interactions, P815 cells were transfected to express human MICA, a ligand for the NK cell activating receptor NKG2D. Transfectants were selected for different levels of surface MICA and quantified by flow cytometry, and different protein levels were confirmed by Western blot analysis (Fig. S2 *A*–*C*).

After 45 min of coculture, $2.4 \pm 0.3\%$ of NKL cells formed nanotubes with untransfected P815, whereas $4.2 \pm 0.5\%$, $11.4 \pm 2.3\%$, and $16.2 \pm 2.4\%$ NKL cells formed nanotubes with P815 transfectants expressing a mean of 1,900, 100,000, and 430,000
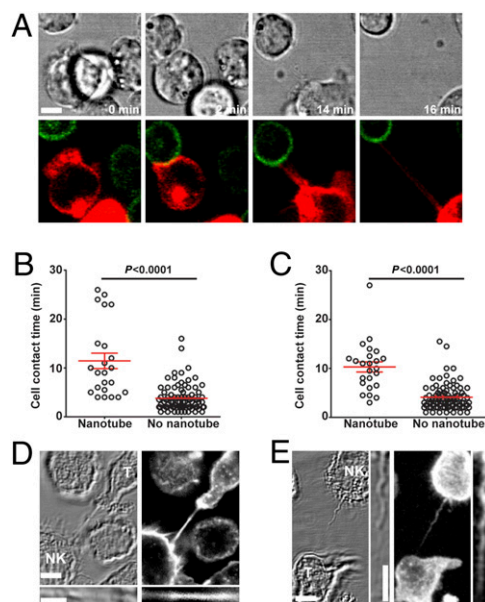

Fig. 2. Characteristics of human NK cell membrane nanotubes. (*A*) Time-lapse microscopy reveals the formation of a nanotube between NKL labeled with membrane dye DiD (red) and P815/MICA-YFP (green, *n* > 100). Images acquired by time-lapse microscopy of primary NK cells (*n* = 109) (*B*) and NKL cells (*n* = 110) (*C*) coincubated with P815/MICA-YFP were analyzed to record the length of time of contact between cells and then whether or not membrane nanotubes formed as cells departed. Cocultures of NKL (labeled NK) and P815/MICA-YFP (labeled T for target cell) were fixed and stained with phalloidin-Alexa633, which marks f-actin (white, *n* > 100) (*D*) or anti-α-tubulin (*E*), followed by secondary mAb conjugated to Alexa633 (white, *n* = 78). Thin panels show an enlarged view of the nanotube. (Scale bars: 10 μm.)

MICA proteins, respectively (Fig. 3*A*). Blockade of NKG2D with mAb abrogated nanotube formation, with transfectants expressing high levels of MICA (Fig. S2*D*), confirming this increase was caused by recognition of MICA by NKG2D. Similarly, $3.6 \pm 0.5\%$ of primary human NK cells formed nanotubes with untransfected P815 cells, and this increased to $5.2 \pm 0.8\%$, $6.1 \pm 0.2\%$, and $9.8 \pm 0.9\%$ for P815 transfectants expressing the increasing levels of MICA (Fig. 3*B*). Thus, not only the presence but the expression level of ligand was important in determining the frequency of NK cell nanotubes. Expression of MICA in 221 also formed nanotubes with NK cells more frequently (Fig. S2*E*). In addition, expression of ICAM-1 in P815 facilitated a 5-fold increase in nanotube formation with NKL cells only when NKL cells were treated with manganese to trigger the conformation of LFA-1, which has high affinity for ICAM-1 (Fig. 3*C*). Thus, the number of receptor/ligand interactions directly influences nanotube formation, and/or there are specific intracellular signals from receptors, such as LFA-1 or NKG2D, that increase nanotube formation.

Signaling by NKG2D occurs via phosphorylation of a YINM motif in the transmembrane adaptor protein DAP10, which recruits PI3K and Grb2 and, in turn, Vav-1 (4, 18–20). Thus, we next transfected NKL to express either WT DAP10 or a mutant of DAP10 in which phenylalanine was substituted for the tyrosine in the YINM motif, with GFP added at the C terminus [NKL/DAP10-GFP or NKL/DAP10(Y85F)-GFP]. The level of surface expression of NKG2D was unchanged in transfectants expressing DAP10(Y85F)-GFP or WT DAP10-GFP, and cytotoxicity was not impaired generally because both transfectants were similarly able to lyse 221, which is killed independent of NKG2D-mediated recognition (Fig. S3 *A* and *B*). However, expression of DAP10(Y85F)-GFP acted as a dominant negative for NKG2D-mediated signaling, because lysis of P815/MICA cells by NKL/DAP10(Y85F)-GFP was dramatically reduced in
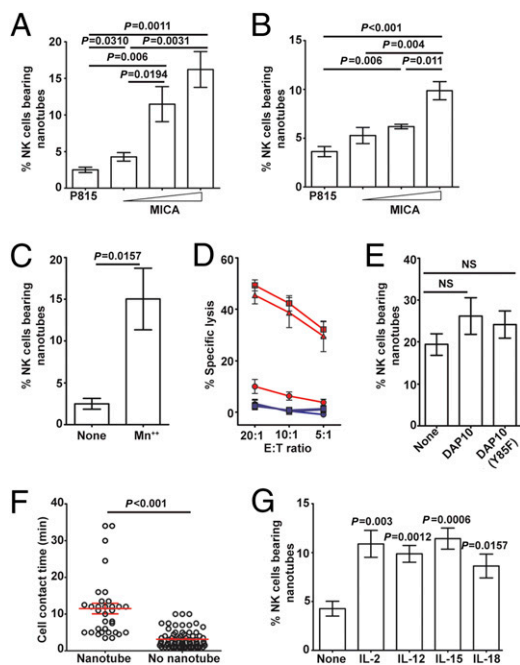
Fig. 3. Frequency of membrane nanotube formation. The frequency at which NK cells formed nanotubes was assessed for cocultures of NKL (*A*) or primary NK (*B*) cells and untransfected P815 or transfectants of P815 expressing different levels of MICA-YFP. (*C*) Frequency at which NKL cells formed nanotubes with transfectants of P815 expressing human ICAM-1 in the presence or absence of manganese (denoted Mn++ or none). (*D*) Untransfected NKL (□) and NKL transfected to express WT DAP10-GFP (△) or DAP10(Y85F)-GFP (○) were each tested for their ability to lyse P815 (blue) or P815/MICA-YFP (red) target cells at different E/T ratios. Data are representative of three independent experiments performed in triplicate. (*E*) These same NK cell lines and transfectants were assessed for the frequency at which they formed nanotubes with P815/MICA-YFP (*n* = 8 experiments). (*F*) Time-lapse microscopy of NKL/DAP10(Y85F)-GFP coincubated with P815/MICA-YFP was analyzed to record the length of time of contact between cells and whether or not membrane nanotubes formed. (*G*) Freshly isolated human NK cells were incubated with different cytokines as indicated and assessed for the frequency at which they made nanotubes with P815/MICA-YFP (*n* = 5 experiments). *P* values shown are in comparison with unstimulated cells.

comparison to untransfected NKL or transfectants of NKL expressing WT DAP10-GFP (Fig. 3*D*). Nevertheless, the frequency of nanotubes formed by NKL expressing signaling-deficient DAP10(Y85F)-GFP with P815 transfectants expressing the highest levels of MICA was the same as that formed by untransfected NKL cells or transfectants of NKL expressing WT DAP10-GFP (Fig. 3*E*). Also, the time required for nanotube formation was not influenced by the reduction in DAP10-mediated signaling because the average contact time that led to nanotube formation was similar for cells expressing DAP10(Y85F)-GFP and untransfected cells (Figs. 3*F* and 2*C*). Thus, although a detailed mechanism for nanotube formation remains to be elucidated, these data establish that the number of receptor/ligand interactions between cells can influence nanotube formation independent, to some extent, of specific signals induced.

Cytokines, including IL-2, IL-12, IL-15, and IL-18, are well known to stimulate NK cell effector responses (21); thus, we next tested their influence on nanotube formation. Human NK cells were isolated and then incubated for 24 h with IL-2, IL-12, IL-15, or IL-18, which increased expression of CD69, indicating cellular activation (Fig. S4*A*). These activated NK cells formed at least twice as many nanotubes with P815/MICA-YFP in comparison to unstimulated NK cells, but there was no significant difference for NK cells activated by different cytokines (Fig. 3*G*). The level

of expression of NKG2D was increased by IL-2, IL-12, IL-15, or IL-18 (Fig. S4*B*), and mAb blocking of NKG2D abrogated the increased frequency of nanotube formation caused by cytokines (Fig. S4*C*). Thus, one way by which cytokines could increase nanotube formation is by increasing expression of NKG2D.

Accumulation of MICA at Nanotube Junctions. We next set out to test whether or not nanotubes could facilitate interactions between NK cells and target cells over long distances. Strikingly, MICA-YFP was readily seen accumulated in over 70% of junctions in nanotubes connecting NK cells to P815/MICA-YFP (Fig. 4 *A* and *B* and Fig. S5 *A–C*). The fluorescence intensity of MICA-YFP was enriched 7.4 ± 0.7-fold compared with MICA-YFP at the surface of the target cell body (Fig. 4*C*). This dramatic enrichment was not attributable to an accumulation of membrane, because YFP tethered to the membrane by palmitoylation (mem-YFP) was not similarly enriched at nanotube junctions (Fig. 4*C*). Time-lapse microscopy of NKL and P815/MICA-YFP revealed that MICA accumulation at the junction could occur either before or after the formation (40% of cases) of the nanotube (*n* > 100) (Fig. 4 *D–F*) and accumulation of MICA at the junction could persist for at least 1 h (Fig. 4*G* and Movie S2).

To assess whether an accumulation of MICA at the small-sized nanotube junction could be sufficient to trigger NK cell activation, we next estimated the number of MICA proteins required to trigger NK cell cytotoxicity. For this, P815 transfectants expressing different quantified amounts of YFP-tagged MICA (Fig. S2 *A–C*) were assessed for lysis by primary human NK cells at different effector/target (E/T) ratios. Transfectants expressing a mean of ≥ 2,000 MICA molecules at the cell surface triggered a cytolytic response, irrespective of the E/T ratio (Fig. 4*H*). Only a fraction of the surface MICA would accumulate at a synapse (e.g., ∼15% of surface class I MHC protein accumulates at NK cell synapses) (22), suggesting a crude estimate of ∼300–2,000 MICA proteins being required to trigger NK cell activation.

To estimate the number of MICA proteins at a nanotube junction, the fluorescence from an individual cell image was quantified and compared with a histogram of fluorescence intensities for many cell images in the population (*n* = 185). This placed the fluorescence from an individual cell at a specific point within the distribution of fluorescence for the population of cells. The fluorescence distribution across cell images could be correlated to the fluorescence distribution obtained by flow cytometry, and this allowed an estimation of the number of MICA proteins expressed by a particular cell being imaged. The fold increase in fluorescence at the nanotube junction could then be used to estimate the number of MICA proteins at that junction. This approach estimated that 4,700 ± 389 MICA proteins accumulated at nanotube junctions (Fig. 4*I*), which is significantly greater than our estimate of the amount of MICA needed to trigger NK cell cytotoxicity at conventional synapses.

Accumulation of DAP-10, Vav-1, and Tyrosine-Phosphorylated Proteins at Nanotube Junctions. To test whether the signaling adaptor DAP10 was recruited to nanotube junctions, NKL/DAP10-GFP was labeled with membrane dye 1,1′dioctadecyl-3,3,3′,3′ tetramethylindodicarbocyanine perchlorate (DiD) before coincubation with the myeloid cell line THP-1 that endogenously expresses MICA. DAP10-GFP was readily seen accumulated at 73.5 ± 2.8% of nanotube junctions (*n* = 92) without there being an analogous accumulation of membrane marked by DiD (Fig. 5*A*). There was a 9.4 ± 1.2-fold enrichment of DAP10-GFP at nanotube junctions in comparison with elsewhere along the nanotube and only a 1.2 ± 0.2-fold increase of NK cell membrane marked by DiD (Fig. 5*B* and Fig. S6*A*). There was no significant recruitment of mem-YFP, further confirming that recruitment of DAP10-GFP was specific (Fig. 5*C* and Fig. S6*B*). DAP10-GFP also accumulated at nanotube junctions with P815/MICA (Fig. S6*C*), confirming that these data
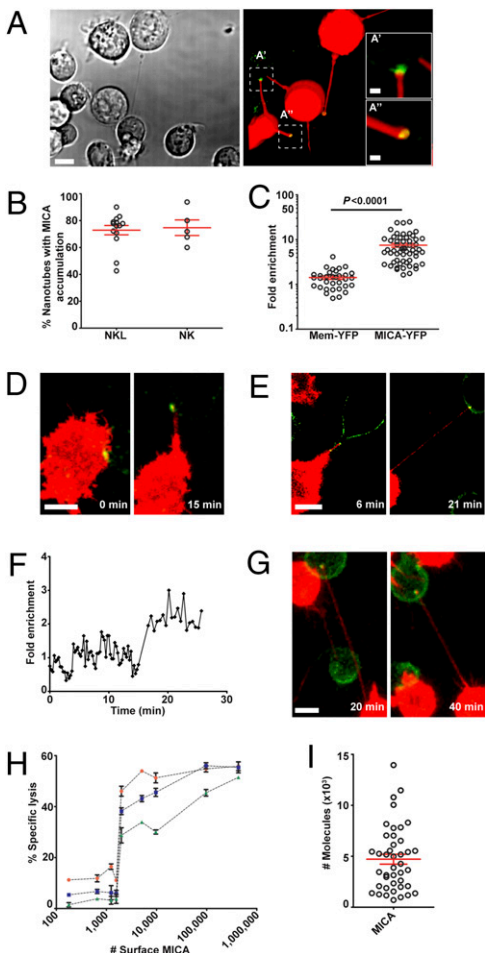
Fig. 4. Accumulation of activating NK cell protein MICA at nanotube junctions. (*A*) Bright-field image with the corresponding fluorescence of NKL (labeled with DiD, red) and P815/MICA-YFP, where MICA-YFP (green) has accumulated at nanotube junctions. This particular field of view is chosen to show several nanotubes, and boxed regions (A′, A″) have been enlarged to allow better visualization of the accumulation of MICA-YFP. (*B*) Frequency of nanotubes wherein MICA accumulated for NKL (*n* = 14 independent experiments) and primary NK cells (*n* = 5 independent experiments) in coculture with P815/MICA-YFP. (*C*) Fold increase of MICA-YFP or mem-YFP at the nanotube junction was measured in comparison to the plasma membrane of the target cell body. Time-lapse microscopy of NKL (red) and P815/MICA-YFP (green) reveals that MICA accumulation can occur either before (*D*) or after (*E*) the formation of membrane nanotubes. Fold increase of MICA-YFP at the nanotube junction (*F*) vs. time for the nanotube shown in *E*, starting from when the nanotube first forms (*t* = 0). (*G*) Time-lapse microscopy shows MICA persists at nanotube junctions for long times. (*H*) Primary human NK cells were tested for lysis of P815 transfectants expressing different mean amounts of MICA at the surface, as quantified by flow cytometry. Percent specific lysis is shown plotted against the mean number of MICA proteins expressed by each target cell transfectant for E/T ratios of 2:1, 1:1, and 0.5:1 (red circles, blue squares, and green triangles, respectively). Error bars are SD of triplicates from a representative sample of 3 independent experiments. (*I*) Number of MICA proteins accumulated at individual nanotube junctions, estimated by correlating the distribution in fluorescence among cells observed by microscopy and flow cytometry (*n* = 41). [Scale bars: 10 μm (inserts: 2 μm).]

were not specific to one type of target cell. For this target cell, there was a striking 16.4 ± 2.9-fold enrichment of DAP10-GFP at junctions and only a 2 ± 0.3-fold increase of NK cell membrane marked by DiD (Fig. S6*D*).

Using NKL and P815/MICA-YFP that were fixed and stained with a mAb specific for tyrosine-phosphorylated residues, a large
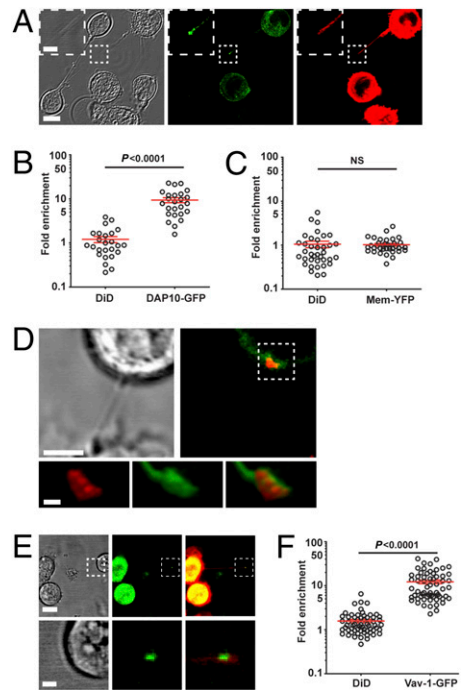

Fig. 5. Accumulation of DAP-10, Vav-1, and tyrosine-phosphorylated proteins at nanotube junctions. (*A*) Representative micrograph (*n* > 100) shows NKL transfected to express DAP10-GFP (green) labeled with membrane dye DiD (red), which is connected to THP-1 (*Lower Left* in bright-field image) via a nanotube. Panels show the bright-field image of cells and the corresponding fluorescence of DAP10-GFP (green) and DiD (red). Also evident in this image is a membrane connection between two THP-1 cells (shown in the bright-field image; not fluorescent). Using transfectants of NKL expressing DAP10-GFP or mem-YFP and THP-1, the fold increase at nanotube junctions of DAP10-GFP and DiD (*n* = 25) (*B*) or mem-YFP and DiD (*n* = 37) (*C*) was measured in comparison with that elsewhere along the nanotube. (*D*) NKL coincubated with P815/MICA-YFP was fixed and stained for phosphotyrosine (red). The boxed region is shown enlarged to allow better visualization of the accumulation of phosphotyrosine (red) along with MICA-YFP (green, *n* = 20). (*E*) Representative micrograph shows NKL transfected to express Vav-1 tagged with GFP, stained with DiD (red), and cocultured with P815/MICA. Panels show the bright-field image and corresponding fluorescence of Vav-1-GFP (green) and an overlay (*Right*, *n* = 60). The boxed regions are shown enlarged in lower panels to visualize the nanotube junction better. (*F*) Using transfectants of NKL expressing Vav-1-GFP and P815/MICA, the fold increase at nanotube junctions of Vav-1-GFP and DiD was measured in comparison with that elsewhere along the nanotube. [Scale bars: 10 μm (inserts: 2 μm).]

accumulation of tyrosine-phosphorylated proteins was also evident at nanotube junctions (*n* = 20) (Fig. 5*D*). Moreover, using NKL transfected to express Vav-1-GFP, accumulation of Vav-1 was readily detected at 64.3 ± 5.9% of nanotube junctions (*n* = 100) (Fig. 5*E*). Enrichment of Vav-1-GFP was 12.2 ± 1.1-fold compared with elsewhere along the nanotube, which was far greater than the 1.5 ± 0.1-fold increase in membrane marked by DiD (Fig. 5*F*). Hence, proximal signaling proteins are recruited to nanotube junctions, suggesting that submicrometer scale immune synapses form at such junctions.

NK Cell Membrane Nanotubes Aid the Lysis of Distant Target Cells.
Strikingly, target cells tethered via a nanotube could move along the nanotube path to form a tight contact with the NK cell body (Fig. 6*A* and Movies S3 and S4). The average speed of 14.3 ± 1.3 μm·min^{-1} at which the target cell moved along the nanotube path was significantly greater than that cell type's speed of migration when moving freely, 8.3 ± 0.6 μm·min^{-1} (Fig. 6*B*). In addition, as target cells moved along the nanotube path, they were commonly polarized (65 ± 5.4%, *n* = 60) such that their
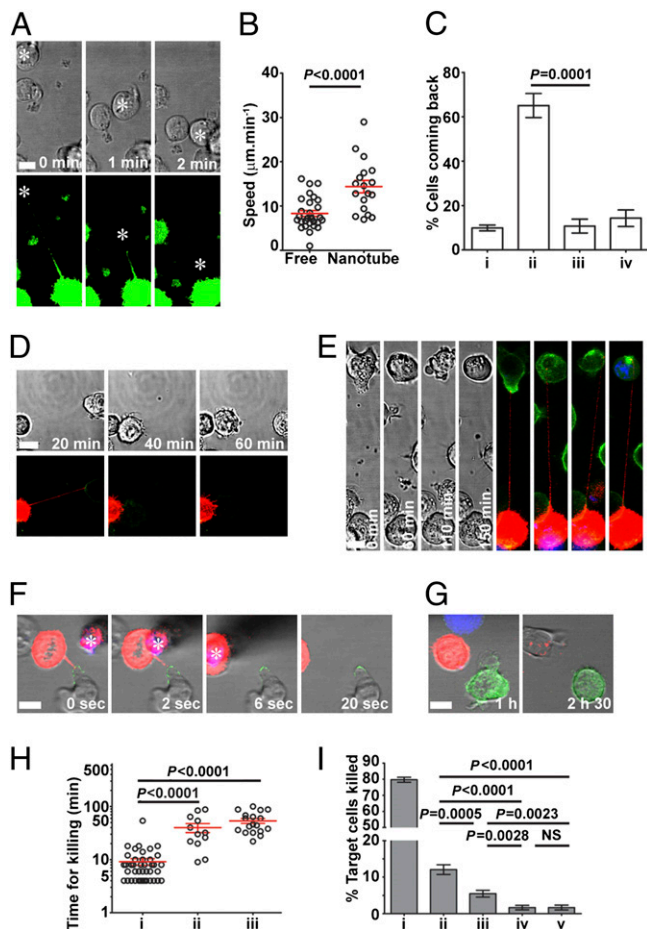
Fig. 6. Functional consequences for membrane nanotubes formed by NK cells. (*A*) Representative example of time-lapse microscopy of NKL/mem-YFP (green) and P815/MICA connected by a membrane nanotube, where the target cell is moved back into close contact with the NK cell (*n* > 60). (*B*) Speed of target cell movement was compared for target cells (P815/MICA or P815/MICA-YFP) freely migrating unidirectionally or moving via a nanotube. (*C*) Orientation of target cell polarity in the direction of movement was scored for target cells (P815/MICA or P815/MICA-YFP) moved toward NKL via nanotubes (*n* = 60). Each target cell was scored as either being (*i*) unpolarized, having its (*ii*) uropod or (*iii*) leading edge facing the direction of movement, or (*iv*) polarized such that neither the leading edge nor the uropod faced the direction of movement. (*D*) Representative time-lapse microscopy shows an example in which a 221/MICA-YFP target cell (green) is moved back along the nanotube path into close contact with NKL stained with DiD (red) and is subsequently lysed as evidenced by membrane blebbing (at 60 min). (*E*) Time-lapse microscopy of 221/MICA-YFP (green) target cells connected to NKL stained with DiD (red) in the presence of DNA dye (blue). Incorporation of the DNA dye was observed at later time points, indicating cell death (*n* = 30). (*F*) Time-lapse fluorescence micrographs of single optical slices show an example of how a nanotube was removed by moving the DiD-labeled (red) NK cell away using a 7-μm needle (starred and red attributable to autofluorescence). (*G*) Time-lapse micrographs of reconstructed z-stacks show how the target cell shown in *F* (221/MICA-YFP, green) was followed after nanotube removal to determine whether or not lysis occurred (i.e., whether or not it stained with a DNA dye, Sytox-blue). (*H*) Time required for DNA dye incorporation following initial intercellular contact was determined for three different processes: (*i*) cell death occurring at a conventional (i.e., large) cytolytic synapse, (*ii*) cell death occurring while the target cell was tethered to a distant NK cell, and (*iii*) cell death occurring after the target cell has come back to the NK cell body via a nanotube. (*I*) Relative frequency of different processes that led to death of 221/MICA target cells was assessed by analysis of a series of 2-h long movies (*n* > 400). Events were scored as death (detected by DNA dye incorporation) occurring (*i*) at a tight cell/cell contact (i.e., via a conventional immune synapse), (*ii*) when target cells were connected to NK cells by nanotubes and had moved back to reform a tight contact, (*iii*) when target cells were connected to a distant NK cell via a membrane nanotube, (*iv*) when target cells had previously been in contact with an NK cell and subsequently moved apart without remaining connected by a nanotube, or (*v*) when cells spontaneously died without interaction with an NK cell. (Scale bars: 10 μm.)

uropods faced the direction of movement (Fig. 6*C* and Fig. S7). This is the opposite orientation of a cell's polarization compared with polarization for normal cell migration. Thus, nanotubes can drive target cells to reform a close contact. Target cells that were moved along the nanotube path to reform a tight contact could be killed subsequently via a cytolytic synapse (Fig. 6*D* and Fig. S7).

In addition, target cells could become lysed while connected to a distant NK cell via a nanotube. One example depicted in Fig. 6*E* and Movie S5 shows NKL coincubated with 221/MICA-YFP in the presence of a DNA dye, Sytox-blue, which becomes integrated in the nucleus of dying cells following the destruction of nuclear membrane integrity. 221/MICA-YFP was initially polarized and lacked DNA staining, but after 60 min, the target cell has lost its polarization and is more granular (Fig. 6*E*). By 110 min, its surface membrane has blebbed, and by 150 min, there is a loss of nuclear membrane integrity observed by integration of the DNA dye. To test directly whether or not nanotubes can facilitate target cell lysis, we compared the frequency at which target cells were killed when connected by a nanotube and left alone or when the nanotube was deliberately removed using a micromanipulator either to move the NK cell away or to sever the nanotube directly (examples shown in Fig. 6 *F* and *G* and Movies S6 and S7). Strikingly, 75% (12 of 16) of target cells that remained connected to an NK cell by a nanotube were lysed, whereas cutting the nanotube reduced lysis of these target cells to 22% (4 of 18). The mechanism by which nanotubes directly aid NK cell-mediated killing is unknown but could involve perforin, because we observed perforin within NK cell nanotubes (Fig. S6 *E* and *F*), or it could involve signals from death-domain receptors at the nanotube synapse.

One consequence of lysis occurring via different processes is that it takes different times. The average time for target cell lysis, as detected by DNA staining, was 9.1 ± 1.3 min for lysis via a conventional synapse, 39.9 ± 7.7 min for lysis of distant target cells connected by a nanotube, and 53.7 ± 5.6 min when the target cell came back to the NK cell along the nanotube path (Fig. 6*H*).

To assess the relative frequency of these processes that lead to target cell death, cells that became stained by DNA dye were traced back through time-lapse micrographs so that the process leading to their death was visualized. In the majority of cases, integration of DNA dye occurred at a large intercellular synapse (Fig. 6*I*). However, ~12% of target cell death occurred when target cells were connected to NK cells by nanotubes and moved back to reform a large synapse. In addition, ~5.4% of target cell death occurred while the target cell was connected to a distant NK cell via a nanotube. Earlier studies using time-lapse imaging showed that cytotoxic T lymphocytes can completely separate from an immobilized target cell before target cell death (23). Such events accounted for very little (<2%) target cell death in our conditions, however. The relative frequency of these processes that lead to death was very similar for another target cell, Daudi transfected to express MICA (Fig. S8). Thus, for this NK cell line and lymphocyte transfectants expressing MICA, nanotubes were involved in ~17% of target cell death.

Discussion

Here, we report characteristics of membrane nanotubes formed by NK cells. Our data suggest that NK cell nanotubes can support submicron scale immune synapses and demonstrate that nanotubes can aid cytotoxicity. The importance of NK cell-mediated cytotoxicity is well established for defense against many infections (24). In addition, NK cell cytotoxicity may be

IMMUNOLOGY

important in removing self-immune cells to prevent excessive inflammatory responses (25). Thus, the data presented here beg the question as to what could be the importance of nanotubes in aiding such cytolytic responses.

It is well established that T or NK cells receive a "stop" signal when activated by a target or antigen-presenting cell (4, 6, 26, 27). However, target cells would not receive an equivalent stop signal; therefore, particularly motile target cells may be able to move away from cytolytic NK or T cells before an effector response has been realized. Hence, one speculative role for nanotubes could be to facilitate cytolytic cells being able to sustain an interaction with target cells that are particularly motile (e.g., other lymphocytes). Another speculative role for nanotubes could be in allowing effector cells to patrol a number of target cells simultaneously such that they interact with one cell while keeping an interaction with a previously encountered cell. Indeed, it has previously been shown that T cells can simultaneously interact with multiple cells presenting different levels of antigen such that they eventually engage fully with the strongest stimulus (28). Membrane nanotubes could aid such a process by maintaining contacts and eventually bringing back an initially encountered target or antigen-presenting cell.

Broadly, it remains to be established how important membrane nanotubes are during specific immune responses. Because nanotube formation is intrinsically linked to cell motility and the duration of intercellular contacts, the frequency of nanotubes formation will vary according to the activation state of cells and the local microenvironment. Here, we found that the frequency at which NK cells form membrane nanotubes was increased by various cytokines. This suggests that nanotubes are more frequently formed by activated cells, consistent with observations in vivo, wherein dendritic cells in the mouse cornea formed more nanotubes on stimulation with LPS or mechanical injury leading to inflammation (29). In summary, the data presented here demonstrate that membrane nanotubes can aid immune cell functions, such as cell-mediated cytotoxicity.

Materials and Methods

For details regarding cells and constructs, antibody staining/blocking, quantification of proteins/fluorescence, and statistical analysis, see *SI Text*.

Live-Cell Imaging. Cells were imaged in eight-well chambered coverglasses (Chambered Borosilicate Coverglass; Lab-Tek) precoated with 10 μg·mL^{-1} fibronectin (Sigma). Cells were imaged at 37 °C, 5% (vol/vol) CO_2 by resonance laser scanning confocal microscopy (TCS SP5 RS; Leica) using excitation wavelengths of 405, 488, 514, and 633 nm with either a 20× dry objective (N.A. = 0.5) or a 63× water immersion objective (N.A. = 1.2) and analyzed (Volocity; Improvision and Image J; National Institutes of Health). To determine nanotube frequency, 40,000 NKL or primary NK cells were labeled with 2 μM DiD according to the manufacturer's instructions and incubated with either 40,000 NK cells stained with 2 μM DiO or 40,000 target cells for 45 min. To analyze nanotube formation, NK cells were incubated with target cells and time-lapse microscopy was performed over 2 h, with a series of confocal slices being acquired every 0.5 min. To image target cell death, 20,000 NK cells labeled with DiD were added to 50,000 target cells in the presence of 0.5 μM Sytox-blue (Invitrogen) and time-lapse microscopy was performed over 2 h with a series of confocal slices being acquired every 1 min. Brightness and contrast were changed in some images, and some bright-field images were "embossed" (Adobe Photoshop) only to increase visibility of nanotubes for publication.

1. Lanier LL (2008) Up on the tightrope: Natural killer cell activation and inhibition. *Nat Immunol* 9:495–502.
2. Raulet DH, Guerra N (2009) Oncogenic stress sensed by the immune system: Role of natural killer cell receptors. *Nat Rev Immunol* 9:568–580.
3. Davis DM, et al. (1999) The human natural killer cell immune synapse. *Proc Natl Acad Sci USA* 96:15062–15067.
4. Orange JS (2008) Formation and function of the lytic NK-cell immunological synapse. *Nat Rev Immunol* 20:713–725.
5. Krzewski K, Strominger JL (2008) The killer's kiss: The many functions of NK cell immunological synapses. *Curr Opin Cell Biol* 20:597–605.
6. Culley FJ, et al. (2009) Natural killer cell signal integration balances synapse symmetry and migration. *PLoS Biol* 7:e1000159.
7. Bryceson YT, Long EO (2008) Line of attack: NK cell specificity and integration of signals. *Curr Opin Immunol* 20:344–352.
8. Davis DM, Sowinski S (2008) Membrane nanotubes: Dynamic long-distance connections between animal cells. *Nat Rev Mol Cell Biol* 9:431–436.
9. Rustom A, Saffrich R, Markovic I, Walther P, Gerdes HH (2004) Nanotubular highways for intercellular organelle transport. *Science* 303:1007–1010.
10. Onfelt B, Nedvetzki S, Yanagi K, Davis DM (2004) Cutting edge: Membrane nanotubes connect immune cells. *J Immunol* 173:1511–1513.
11. Gerdes HH, Carvalho RN (2008) Intercellular transfer mediated by tunneling nanotubes. *Curr Opin Cell Biol* 20:470–475.
12. Hase K, et al. (2009) M-Sec promotes membrane nanotube formation by interacting with Ral and the exocyst complex. *Nat Cell Biol* 11:1427–1432.
13. Onfelt B, et al. (2006) Structurally distinct membrane nanotubes between human macrophages support long-distance vesicular traffic or surfing of bacteria. *J Immunol* 177:8476–8483.
14. Watkins SC, Salter RD (2005) Functional connectivity between immune cells mediated by tunneling nanotubules. *Immunity* 23:309–318.
15. Sowinski S, et al. (2008) Membrane nanotubes physically connect T cells over long distances presenting a novel route for HIV-1 transmission. *Nat Cell Biol* 10:211–219.
16. Gousset K, et al. (2009) Prions hijack tunnelling nanotubes for intercellular spread. *Nat Cell Biol* 11:328–336.
17. Sherer NM, Mothes W (2008) Cytonemes and tunneling nanotubules in cell-cell communication and viral pathogenesis. *Trends Cell Biol* 18:414–420.
18. Wu J, et al. (1999) An activating immunoreceptor complex formed by NKG2D and DAP10. *Science* 285:730–732.
19. Gilfillan S, Ho EL, Cella M, Yokoyama WM, Colonna M (2002) NKG2D recruits two distinct adapters to trigger NK cell activation and costimulation. *Nat Immunol* 3:1150–1155.
20. Diefenbach A, et al. (2002) Selective associations with signaling proteins determine stimulatory versus costimulatory activity of NKG2D. *Nat Immunol* 3:1142–1149.
21. Biron CA, Nguyen KB, Pien GC, Cousens LP, Salazar-Mather TP (1999) Natural killer cells in antiviral defense: Function and regulation by innate cytokines. *Annu Rev Immunol* 17:189–220.
22. Almeida CR, Davis DM (2006) Segregation of HLA-C from ICAM-1 at NK cell immune synapses is controlled by its cell surface density. *J Immunol* 177:6904–6910.
23. Rothstein TL, Mage M, Jones G, McHugh LL (1978) Cytotoxic T lymphocyte sequential killing of immobilized allogeneic tumor target cells measured by time-lapse microcinematography. *J Immunol* 121:1652–1656.
24. Orange JS (2006) Human natural killer cell deficiencies. *Curr Opin Allergy Clin Immunol* 6:399–409.
25. Nedvetzki S, et al. (2007) Reciprocal regulation of human natural killer cells and macrophages associated with distinct immune synapses. *Blood* 109:3776–3785.
26. Dustin ML, Springer TA (1989) T-cell receptor cross-linking transiently stimulates adhesiveness through LFA-1. *Nature* 341:619–624.
27. Davis DM (2009) Mechanisms and functions for the duration of intercellular contacts made by lymphocytes. *Nat Rev Immunol* 9:543–555.
28. Depoil D, et al. (2005) Immunological synapses are versatile structures enabling selective T cell polarization. *Immunity* 22:185–194.
29. Chinnery HR, Pearlman E, McMenamin PG (2008) Cutting edge: Membrane nanotubes in vivo: A feature of MHC class II+ cells in the mouse cornea. *J Immunol* 180:5779–5783.